JOURNAL OF GEOPHYSICAL RESEARCH, VOL. 113, A09213, doi:10.1029/2008JA013322, 2008

AKR breakup and auroral particle acceleration at substorm onset

A. Morioka,[1] Y. Miyoshi,[2] F. Tsuchiya,[1] H. Misawa,[1] K. Yumoto,[3] G. K. Parks,[4] R. R. Anderson,[5] J. D. Menietti,[5] E. F. Donovan,[6] F. Honary,[7] and E. Spanswick[6]

Received 16 April 2008; revised 16 June 2008; accepted 24 June 2008; published 9 September 2008.

[1] The dynamical behavior of auroral kilometric radiation (AKR) is investigated in connection with auroral particle acceleration at substorm onsets using high-time-resolution wave spectrograms provided by Polar/PWI electric field observations. AKR develops explosively at altitudes above a preexisting low-altitude AKR source at substorm onsets. This ''AKR breakup'' suggests an abrupt formation of a new field-aligned acceleration region above the preexisting acceleration region. The formation of the new acceleration region is completed in a very short time (amplitude increases 10,000 times in 30 seconds), suggesting that the explosive development is confined to a localized region. AKR breakups are usually preceded (1–3 minutes) by the appearance and/or gradual enhancement of the low-altitude AKR. This means that the explosive formation of the high-altitude electric field takes place in the course of the growing low-altitude acceleration. The development of the low-altitude acceleration region is thus a necessary condition for the ignition of the high-altitude bursty acceleration. The dH/dt component from a search-coil magnetometer at ground shows that a few minutes prior to substorm onsets, the quasi-DC component begins a negative excursion that is nearly synchronized with the start of the gradual enhancement of the low-altitude AKR, indicating a precursor-like behavior for the substorm. This negative variation of dH/dt suggests an exponentially increasing ionospheric current induced by the upward field-aligned current. At substorm onsets, the decrease in the quasi-DC variation of dH/dt further accelerates, indicating a sudden reinforcement of the field-aligned current.

Citation: Morioka, A., et al. (2008), AKR breakup and auroral particle acceleration at substorm onset, *J. Geophys. Res.*, *113*, A09213, doi:10.1029/2008JA013322.

1. Introduction

[2] Since the auroral substorm concept was first introduced from the ground-based auroral observations [*Akasofu*, 1964], many mechanisms for the magnetospheric substorm have been proposed. One of the most challenging subjects of substorm research is the onset process of substorm expansion, which is the beginning of the violent release of energy into the ionosphere that is stored in the magnetosphere. There are currently two major scenarios for the triggering of a substorm: the near-Earth neutral line (NENL) model [e.g., *Baker et al.*, 1996; *Shiokawa et al.*, 1998] which proposes that magnetic reconnection in the mid-tail initiates substorm onset, and the current disruption (CD) model [e.g., *Lui et al.*, 1992; *Lyons*, 1995] which proposes that cross-tail–current disruption in the near-Earth tail region triggers substorm onset.

[3] In both scenarios, abrupt particle acceleration along auroral field lines is essential to complete the substorm onset process. A sudden formation of a parallel electric field in the magnetosphere-ionosphere (M-I) coupling system is required. However, neither scenarios necessarily contain a self-consistent field-aligned acceleration process; instead, it is a consequence of the process. In these substorm onset arguments, a question arises: Can the ionosphere at any time accept the onset demand from the magnetosphere and instantly build up a parallel electric field in the M-I coupling region? There might be cases in which the ionosphere is not ready for a substorm, not ready to establish a substorm current closure between the magnetosphere and ionosphere and field-aligned acceleration. To answer this question, we need detailed observations of the dynamical behavior (vertical development) of the field-aligned acceleration region around substorm onset times as well as information on the latitudinal and longitudinal expansion of the auroral arcs (horizontal development).

[1] Planetary Plasma and Atmospheric Research Center, Tohoku University, Sendai, Japan.
[2] Solar-Terrestrial Environment Laboratory, Nagoya University, Nagoya, Japan.
[3] Space Environment Research Center, Kyushu University, Fukuoka, Japan.
[4] Space Sciences Laboratory, University of California, Berkeley, California, USA.
[5] Department of Physics and Astronomy, University of Iowa, Iowa City, Iowa, USA.
[6] Department of Physics and Astronomy, University of Calgary, Calgary, Alberta, Canada.
[7] Department of Communication Systems, Lancaster University, Lancaster, UK.

0148-0227/08/2008JA013322$09.00

[4] The existence of auroral particle acceleration parallel to the ambient magnetic field in the upward field-aligned current (FAC) region has been established by sounding rocket observations [e.g., *Evans*, 1974; *Arnoldy et al.*, 1974] and satellite observations [e.g., *Shelley et al.*, 1976; *Mizera and Fennell*, 1977]. Direct evidence of parallel electric fields in the auroral acceleration region was first reported by *Mozer et al.* [1977]. These observations were consistent with the inverted-V particle precipitation [*Frank and Ackerson*, 1971] associated with the auroral arcs. Recent in-situ observations from the Polar and Fast Auroral Snapshot (FAST) satellites revealed detailed characteristics of field-aligned electric fields together with accelerated particle spectra and background plasma distributions therein. These observations suggest that parallel electric fields are located at two altitudes (high-altitude $E_{//}$ and low-altitude $E_{//}$) from about 0.5 to 2 R_E [*Ergun et al.*, 2002]. These in-situ observations have greatly contributed to the understanding of the comprehensive behavior of quasi-steady auroral particle acceleration in the M-I coupling region.

[5] The important issues still to be addressed after these observations are as follows: (1) How does the field-aligned acceleration evolve prior to and at substorm onsets and during substorm expansion phases? (2) What is the connection between substorm triggering in the magnetosphere and the abrupt build up of the auroral particle acceleration in the ionosphere? These questions require knowledge about the time-dependent vertical evolution of the acceleration region at substorm onsets.

[6] AKR remote senses field-aligned acceleration region at substorms because AKR is initiated by the accelerated electrons in the M-I coupling region. *Kaiser and Alexander* [1977] first discussed the substorm evolution and related AKR source dynamics using the AKR spectrograms. Subsequently many studies [e.g., *Morioka et al.*, 1981; *Liou et al.*, 2000; *de Feraudy et al.*, 2001; *Hanasz et al.*, 2001] have addressed the acceleration altitude in the auroral region on the basis of the AKR spectra. *Olsson et al.* [2004] and *Janhunen et al.* [2004] suggested Alfvén waves can accelerate auroral particles on the basis of the AKR spectral characteristics.

[7] *Morioka et al.* [2007] recently derived information on the dynamical behavior of the field-aligned acceleration during substorms using high-time-resolution spectrograms. They assumed that AKR is radiated at the local electron cyclotron frequency in the parallel electric field region and that the frequency-band reflected the source altitude along the auroral field line. They then investigated the evolution of the auroral acceleration region from the AKR spectral behavior and obtained information on the vertical structure of the acceleration region and its dynamic behavior prior to and during a substorm. Dual acceleration regions at substorm onset were identified: a low-altitude one and a high-altitude one. The low-altitude acceleration region appeared during the substorm growth phase at 4000 to 5000 km, while the high-altitude one appeared abruptly with the substorm onset at 6000 to 12,000 km.

[8] The high-altitude AKR has been studied in terms of "isolated AKR" (ITKR [*Steinberg et al.*, 1988, 1990]), "different types of AKR" (LF burst [*Kaiser et al.*, 1996; *Desch and Farrell*, 2000]) "dot-AKR" [*de Feraudy et al.*, 2001], and "LF-AKR" [*Olsson et al.*, 2004; *Janhunen et al.*, 2004]. It has generally been agreed that the low-frequency component of AKR is accompanied by substorm onset almost without exception [e.g., *Anderson et al.*, 1997, 1998].

[9] The progress of these observations now enables us to study the connection between the auroral acceleration process and magnetospheric substorm onsets. In this paper, we investigate the detailed dynamics of the M-I coupling region in relation to the substorm onset and discuss how the auroral acceleration region evolves in relation to magnetospheric substorms.

2. Database Used

[10] The Polar satellite is in a highly elliptical polar orbit with an apogee at about 9 R_E, and it collects data from a high-altitude perspective on auroral activities. We used the AKR data provided from Plasma Wave Investigation (PWI) [*Gurnett et al.*, 1995] observations onboard the Polar satellite. PWI provides high-time-resolution spectral data for the electric field every 2.352 seconds, which enables us to investigate the fine evolution of the AKR source along the auroral field lines.

[11] Polar Ultra Violet Imager (UVI) data [*Torr et al.*, 1995] were also used to examine the synoptic auroral activity during substorms. All-sky imager data at Gillam (from the NORSTAR database) were referred in identifying the local breakup of auroral substorms. Geomagnetic pulsation data from auroral (from WDC in NIPR), sub-auroral (from the SAMNET and CAMNOS databases), and low-latitude (from WDC in Kyoto University) stations were used to identify substorm onset by Pi 2 pulsation. The location and related geomagnetic information on these ground stations are listed in Table 1.

3. Observations

3.1. AKR Breakup and Substorm

[12] Since AKR is generated at the local electron cyclotron frequency, f_c, by beamed electrons in the auroral acceleration region [e.g., *Ergun et al.*, 1998; *Delory et al.*, 1998; *Pottelette et al.*, 2001], the altitude range of the AKR source can be estimated from its frequency-band. Thus the *f-t* diagram of AKR can be converted into an altitude-time (*a-t*) diagram of the AKR source [*Morioka et al.*, 2007]. Figure 1a shows the $a-t$ diagram of AKR sources converted from the *f-t* diagram observed by PWI on 30 January 1997. The auroral field line of the AKR emission was assumed to be at $L = 7$ (Invariant latitude (ILAT) = 67.7°). Since f_c is not sensitive to the invariant latitude in the polar region, the estimated AKR altitude is valid even when the auroral field line is not exactly $L = 7$. The right ordinate of Figure 1a shows the observed frequency for reference. The AKR intensity is represented by the false color code in logarithm of AKR power. The periodic structures at around 15,000 and 13,000 km (corresponding to about 40 and 60 kHz, respectively) here and in all of the *a-t* diagrams shown hereafter are instrumental artifacts. Figure 1d presents ULF data at the midlatitude station (Victoria; $L = 2.9$) in the midnight sector. The two Pi 2 pulsations starting around 08:08 and 08:42 UT indicate substorm onsets in the magnetosphere [e.g., *Saito*

Table 1. Station Coordinates Used in This Study[a]

Station	Code	Geographic		Corrected Geomagnetic		*L*-value	MLT MN in UT
		Latitude	Longitude	Latitude	Longitude		
Kakioka	KAK	36.2°	140.2°	29.2°	211.8°	1.3	15:04
Victoria	VIC	48.5°	236.6°	53.68°	296.2°	2.9	8:52
Kvistaberg	KVI	59.5°	17.6°	56.1°	96.0°	3.3	21:50
Nordli	NOR	64.4°	63.4°	60.2°	138.0°	4.1	19:13
Syowa	SYO	−69.0°	35.6°	−65.6°	69.6°	6.0	0:06
Tjornes	TJO	66.2°	342.9°	66.5°	72.3°	6.4	23:45
Gillam	GILL	56.4°	265.4°	66.8°	331.3°	6.5	6:37

[a]Corrected magnetic coordinates are calculated for 1996.

et al., 1976]. From Figures 1a and 1d, we can derive the AKR source dynamics during the substorm. Low-altitude AKR appeared around 08:00 UT at altitudes from 3000 to 6000 km. Almost simultaneously with the first Pi 2 onset at around 08:08 UT, the AKR source region suddenly expanded to a higher altitude. The colored/contoured *a-t* diagram indicates that this source expansion was not a simple development from the preexisting low-altitude

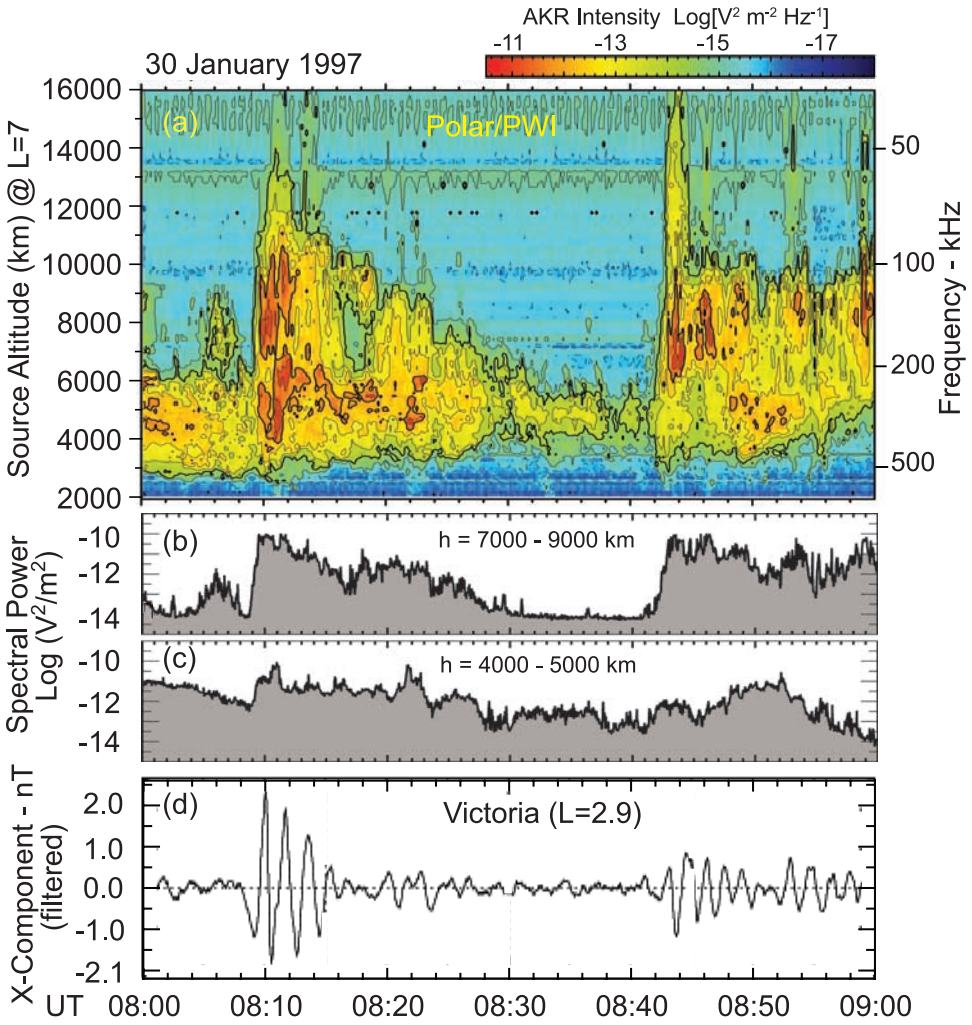

Figure 1. Dual AKR sources (low-altitude and high-altitude AKR) at substorm onset. (a) Altitude-time ($a - t$) diagram of AKR for 1 hour on 30 January 1997, obtained from Polar/PWI observations. The vertical axis is altitude of f_c along field line of $L = 7$. Corresponding frequency is shown on the right ordinate for reference. The periodic structures observed around 15,000 and 13,000 km altitudes (corresponding to about 40 and 60 kHz, respectively) are instrumental interference artifacts. (b) Integrated spectral power of high-altitude AKR for 7000 to 9000 km. (c) Integrated spectral power of low-altitude AKR for 4000 to 5000 km. (d) X-component of geomagnetic pulsation at midlatitude station (Victoria); it indicates two Pi 2 events at around 08:08 and 08:42 UT.

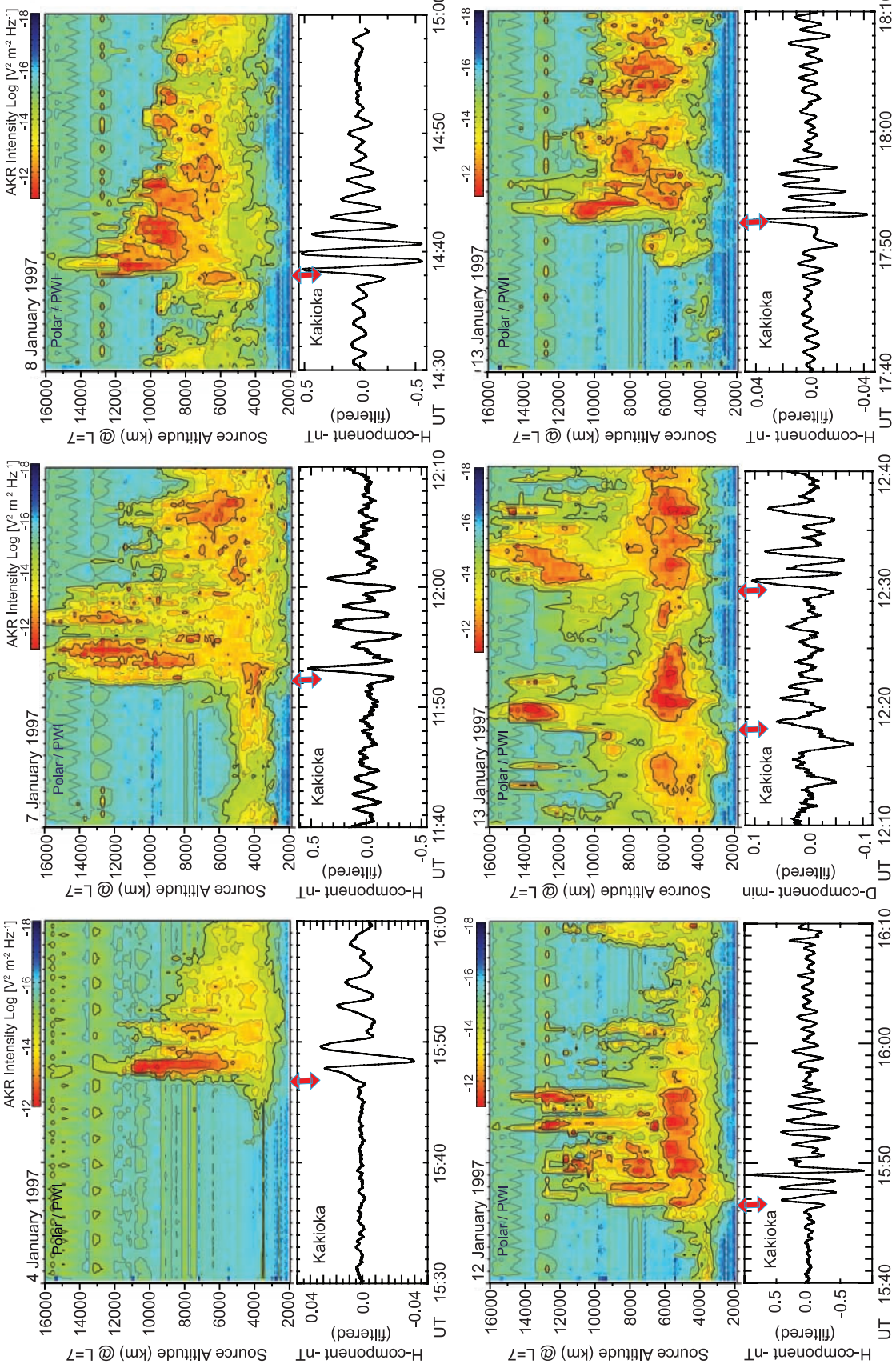

Figure 2. Typical examples of *a-t* diagram of AKR from Polar/PWI and geomagnetic pulsation data at low-latitude station (Kakioka), showing that high-altitude AKR appears above preexisting low-altitude AKR at substorm onsets (onset of Pi 2 pulsation). Six examples are from observations during the first 2 weeks in January 1997.

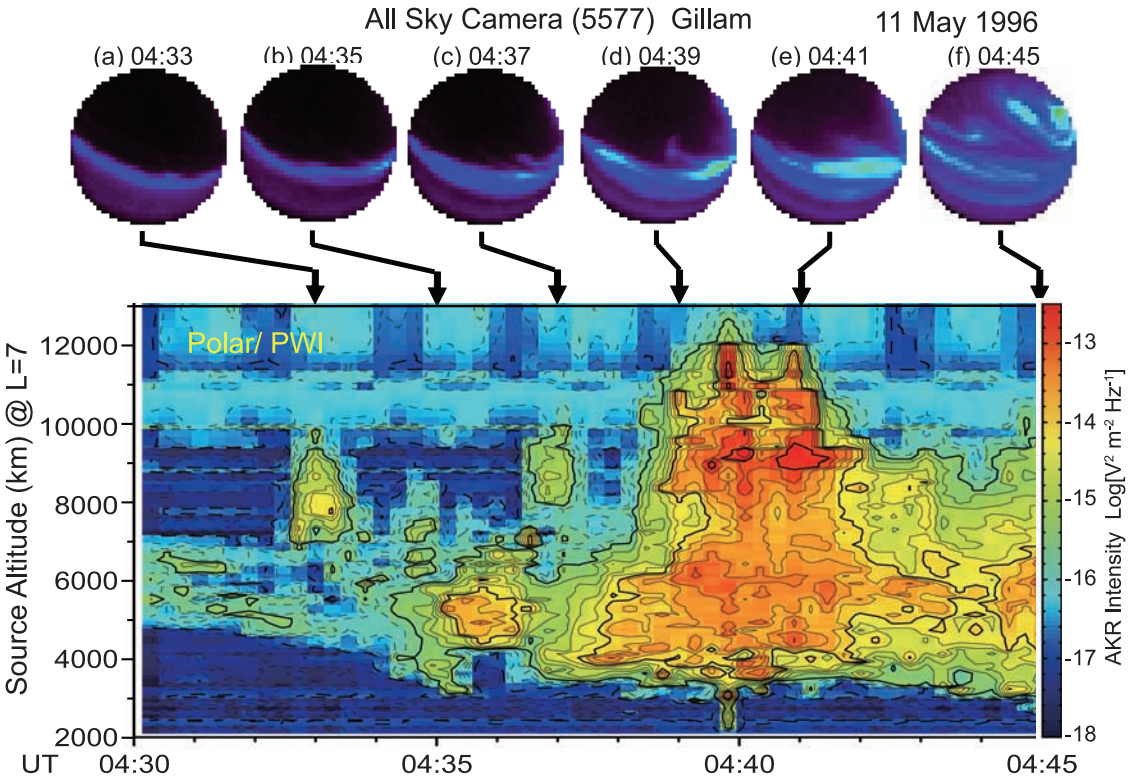

Figure 3. Relationship between local auroral activity and AKR development around the substorm onset. Upper panel: all-sky images from Gillam on 11 May 1996 demonstrating local breakup at 04:39 UT (image d). Lower panel: *a-t* diagram of AKR indicating AKR breakup at 04:39 UT after gradual enhancement of low-altitude AKR.

AKR source but an abrupt appearance of a newly created intense AKR source (high-altitude AKR) above the preexisting one. The altitude of the new high-altitude source ranged from 7000 to 14,000 km. This is the dual structure of the acceleration regions at substorm onset reported by *Morioka et al.* [2007]. By the time of the second substorm onset at ~08:42, the high-altitude AKR had weakened and the low-altitude AKR had decayed into a narrow source at an altitude ~5000 km. Near the second substorm onset, the AKR source region was again activated. Immediately before the second Pi 2 onset (about 1 min before), the low-altitude AKR intensity increased, and an intense high-altitude AKR appeared over a wide altitude range (6500–16,000 km).

[13] Figures 1b and 1c represent the power profiles of the AKR intensity at high altitudes (7000–9000 km) and low altitudes (4000–5000 km), respectively. It is evident from these figures that the high-altitude AKR intensity grew explosively, almost four orders of magnitude within 30 seconds at the 08:08 UT onset and within 1 minute at the 08:42 UT onset. Other cases of fast evolutions of the high-altitude sources at substorm onsets were reported by *Morioka et al.* [2007] (see Figure 6 of their paper). The low-altitude AKR (Figure 1c), on the other hand, grew rather slowly and showed small variations in intensity.

[14] These features of AKR during substorms are commonly observed: a low-altitude AKR source appears prior to and during the substorm over a rather narrow altitude range (4000 to 6000 km in altitude), while a high-altitude AKR source suddenly appears with intense power at the substorm onset along a wider altitude range (6000 to 12,000 km in altitude) above the preexisting low-altitude AKR source. Figure 2 illustrates how often and how similarly Pi 2 associated (substorm associated) AKR is observed. The figure shows *a-t* diagrams of AKR from the Polar satellite and simultaneous ULF data from Kakioka (L = 1.3). These six examples are typical ones found from the data set in the 20–03 h magnetic local time (MLT) at Kakioka during the first 2 weeks in January 1997. All of them demonstrate that high-altitude AKR suddenly appears above preexisting low-altitude AKR at substorm onsets. *Morioka et al.* [2007] indicated that 69% of the associations between AKR and low latitude Pi 2 showed the sudden appearance of a new high-altitude AKR source at substorm onsets.

[15] Here we propose a term "AKR breakup" to describe the abrupt development of the field-aligned acceleration region in the M-I coupling region at substorm onsets.

3.2. AKR Breakup and Auroral Breakup

[16] The relationship between AKR breakup and local auroral breakup is shown in Figure 3. The lower panel shows the *a-t* diagram for 15 min on 11 May 1996. Weak low-altitude AKR was observed between 5000 and 7000 km which gradually decreased. The intensity of the low-altitude AKR increased at ~04:34 UT, and intensified again around 04:37 UT after a modest intensity gap. About 2 minutes after the start of the second gradual increase, high-altitude AKR suddenly appeared and completed its growth within

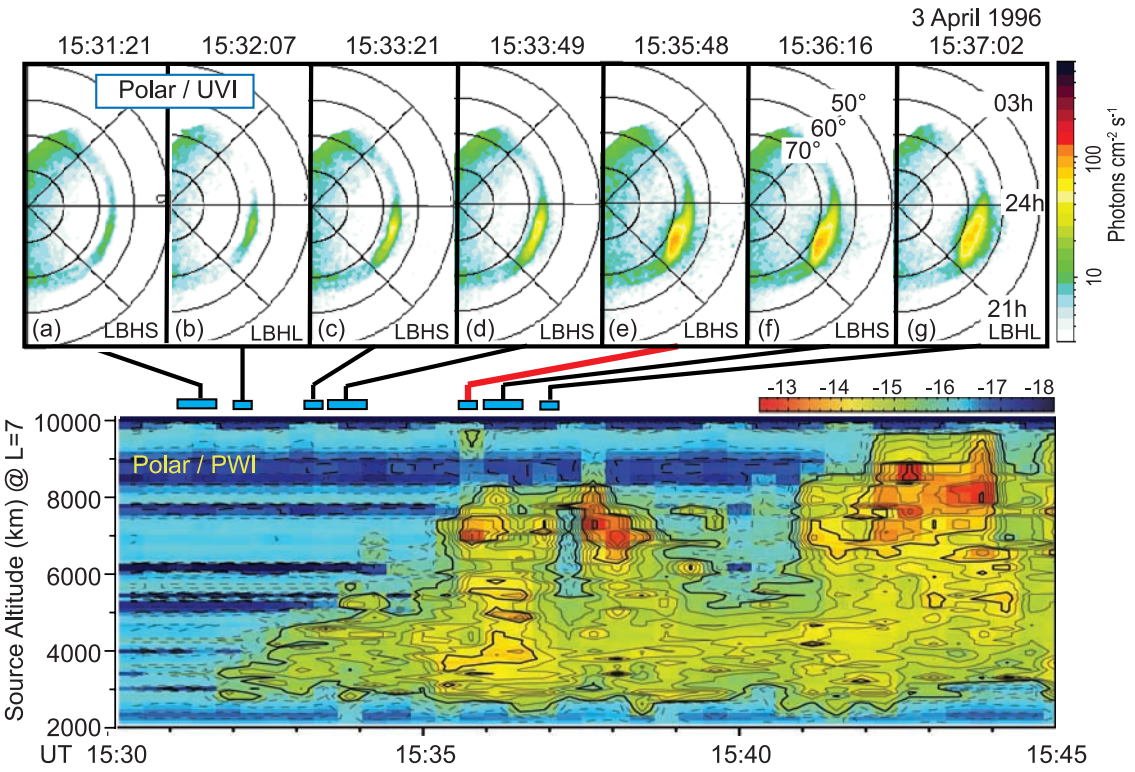

Figure 4. Relationship between global auroral activity and AKR development around a substorm onset. Upper panels: Polar/UVI images in dark hemisphere on 3 April 1996 showing an auroral breakup around 15:35 UT (image e). The small horizontal rectangles under images indicate exposure times. Lower panel: *a-t* diagram indicating AKR breakup at 15:35 UT after gradual enhancement of the low-altitude AKR.

about 30 seconds at altitudes of 8000–12,000 km with peak intensity at 9000 km. This abrupt buildup of the dual sources at 04:39 UT is the AKR breakup. It is again demonstrated that the high-altitude AKR is not an extension from low-altitude AKR but is a newly created source. The upper panel of Figure 3 shows all-sky images from Gillam ($L = 6.5$). A stable auroral arc was observed slightly south of the zenith until 04:35 UT. At 04:37 UT (image c), both the arc brightness and latitudinal extent increased, corresponding to the second intensification of the low-altitude AKR. The auroral arc broke up at 04:39 UT (image d) showing sudden arc intensification and poleward expansion. This observation confirms that AKR breakups coincide with local auroral breakups at auroral latitudes.

[17] Figure 4 shows the relationship between AKR source evolutions and global auroral activities seen from the Polar satellite. The lower panel is the *a-t* diagram on 3 April 1996. Low-altitude AKR appeared at ~15:32 UT in the altitude range 3000–5000 km, and began intensification at ~15:35 UT. Between 15:35 and 15:36 UT, AKR breakup took place showing a formation of a new high-altitude source with the growth time of about 30 seconds. The new high-altitude AKR extended up to 8500 km with peak intensity at ~7000 km. After this AKR breakup, several AKR breakups recurred (~15:38 and ~15:42 UT) at high altitudes, while the low-altitude AKR was relatively inactive. The upper panel of Figure 4 shows a sequence of nightside (1800–0600 MLT) auroral UVI images. The 7 images in the panel are all that were available during this period (15:31 to 15:37 UT). The images were obtained by a combination of LBHL and LBHL filters in the wavelength range 140–180 nm. The narrow blue horizontal bar under each panel indicates the exposure time. The faint oval around 65–67°magnetic latitude in the premidnight sector (image a) gradually became brighter and its latitudinal extent widened (image b), roughly coincident with the appearance of the low-altitude AKR. It became more distinct and clearer and continued to grow (images c and d). The image at 15:35:48 (image e) corresponds to an auroral breakup or immediately after a breakup as shown by the intense brightening at the center of the active region and the poleward expansion of the poleward boundary. This auroral breakup (or the moment immediately after the breakup) was almost simultaneous with the AKR breakup. This confirms that auroral breakup is the time when the local ionosphere in the center of the active region connects to the magnetosphere through a suddenly formed parallel acceleration region.

[18] It should be also noted that, before the auroral breakup, the gradual intensification of the auroral arc/oval started almost concurrently with the appearance of low-altitude AKR (15:32 UT). This tight relationship between the pre-breakup auroral activity and the low-altitude acceleration region suggests that the low-altitude AKR is not directly related to the local breakup but is related to the global intensification of the aurora in the auroral oval.

3.3. Evolution of Acceleration Region and Field-Aligned Current Around Substorm Onset

[19] To elucidate the formation process of the auroral acceleration region at substorm onsets, we further examined

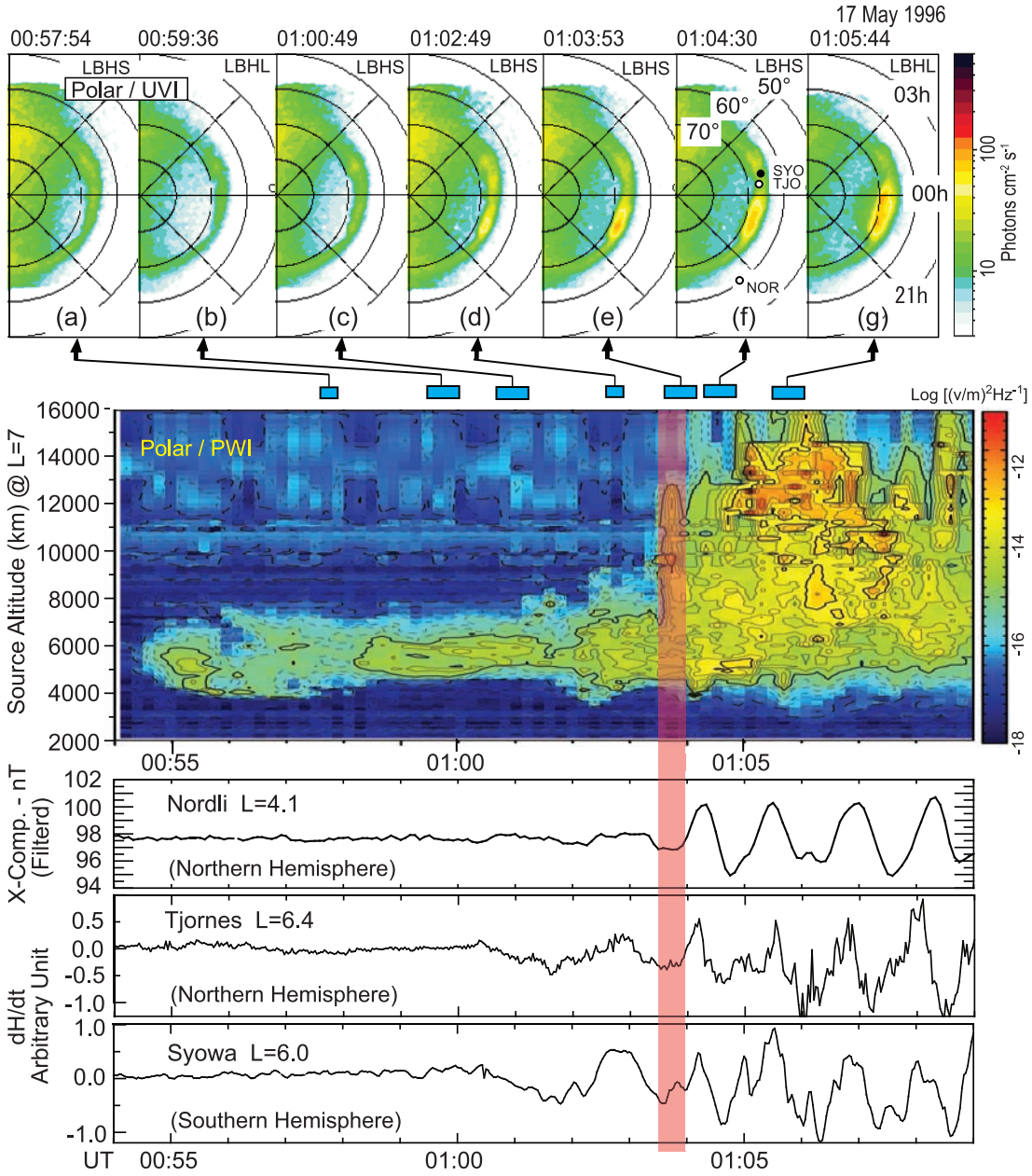

Figure 5. Substorm event on 17 May 1996. (top) UVI images in dark hemisphere demonstrating auroral breakup at 01:03:53 UT (image e). The small horizontal rectangles under the images indicate exposure times. (middle) *a-t* Diagram indicating AKR breakup at around 01:04 UT after gradual enhancement of low-altitude AKR. (bottom) ULF data at Nordli (L = 4.1), Tjornes (L = 6.4), and Syowa (L = 6.0). Locations of ULF stations are shown in image (f) by small circles. The vertical rectangle shows interval of presumed substorm onset.

the relationship between the AKR and FAC evolution during substorm onset using ULF data obtained at auroral and midlatitude stations.

3.3.1. 17 May 1996 Event

[20] The upper two panels in Figure 5 are in the same format as those in Figure 4. They illustrate the Polar observations for the development of an auroral oval and AKR. At around 01:04 UT on 17 May 1996, the AKR broke up almost simultaneously with the auroral breakup. In the UV image at 01:03:53 UT (image e), a bright spot appeared at the center of the active region on the premidnight oval. It is again seen that, before the AKR breakup, weak low-altitude AKR appeared, and its gradual growth was followed by the pre-breakup evolution of the auroral oval. The last three panels plot the ULF data at the midlatitude station (Nordli; L = 4.1) in the northern hemisphere, and geomagnetically conjugate-pair stations at auroral latitudes (Tjornes (L = 6.4) in Iceland and Syowa (L = 6.0) in Antarctica). The local times of these stations during the auroral breakup were dusk (Nordli) and post midnight (Tjornes and Syowa)

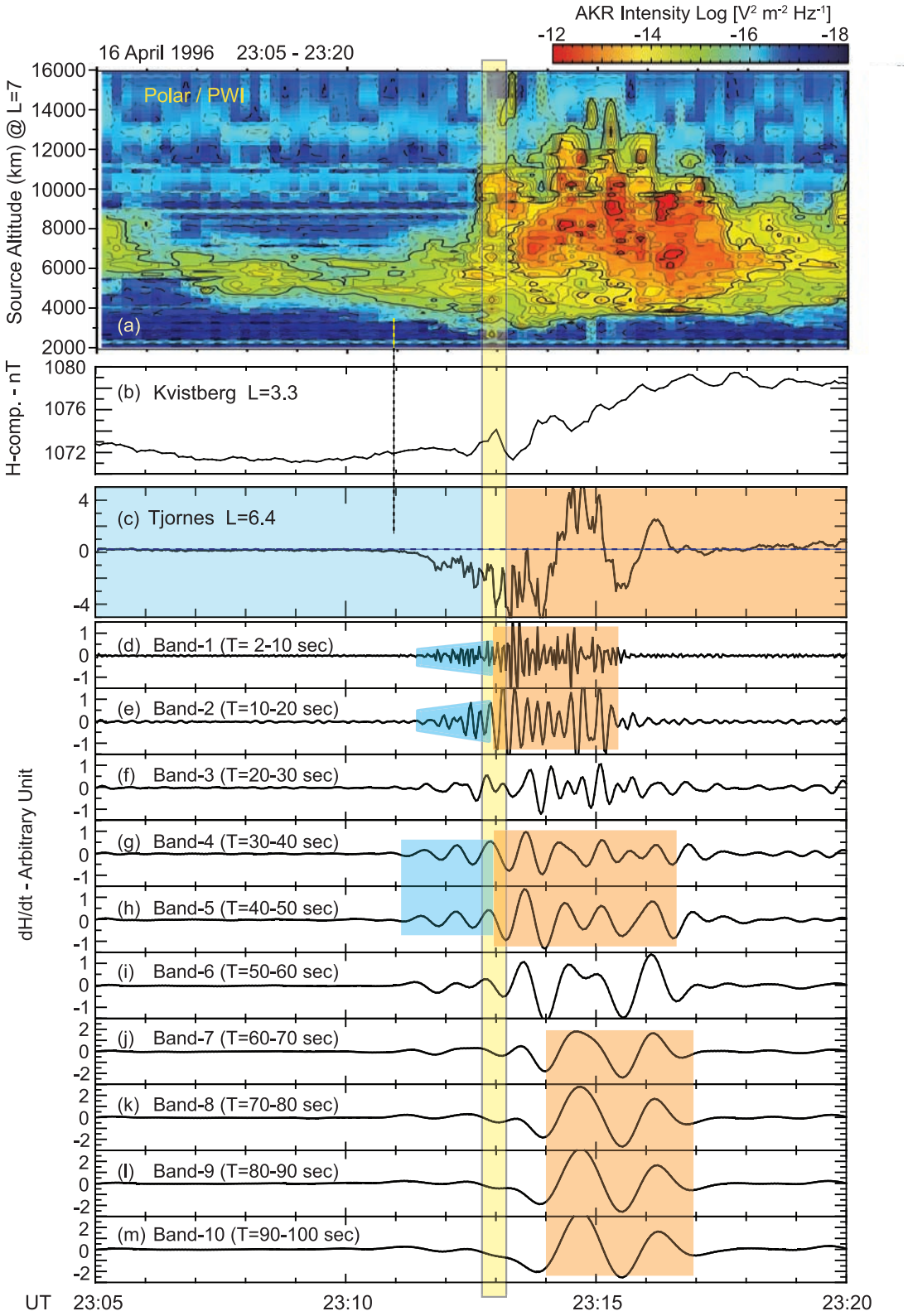

Figure 6. Substorm event on 16 April 1996. (a) *a-t* Diagram indicating AKR breakup at around 23:13 UT after gradual enhancement of low-altitude AKR. (b) Magnetogram at Kvistberg (L = 3.3) indicating midlatitude Pi 2 pulsation at around 23:13 UT. (c) dH/dt data at Tjornes (L = 6.4) indicating high-latitude Pi 2 event from 23:11 to 23:17. (d–m) Band-pass filtered ampligrams of dH/dt signal at Tjornes divided into 10 bands from 2 to 100 seconds. The vertical rectangle shows interval of presumed substorm onset.

(see image f of Figure 5). The Nordli ULF data showed typical Pi 2 pulsation at ~01:04 UT, almost coincident with both auroral and AKR breakups. Low-latitude and midlatitude Pi 2 pulsations are manifestation of magnetospheric substorm onsets [*Yumoto et al.*, 1994; *Olson*, 1999; *Kepko et al.*, 2004] accurate to ~1.5 min on average [*Liou et al.*, 1999; *Meng and Liou*, 2004]. Considering the simultaneous onset of midlatitude Pi 2 with the AKR breakup and auroral breakup, we deduce the substorm onset time to be 01:03:30–01:04:00 UT (indicated by the vertical rectangle in Figure 5).

[21] The ULF data of both auroral conjugate stations showed long-period magnetic field oscillation began at ~01:00 UT, about 3.5 minutes before the substorm onset At substorm onset, a new irregular oscillation, the start of which was almost synchronized with the midlatitude Pi 2 pulsation observed at Nordli, was superposed on the preexisting longer period oscillations. Note that the fundamental components of both pre- and post-onset oscillations were basically in phase between the two conjugate-pair stations and midlatitude station, indicating that they were not locally generated irregular oscillations in the ionosphere but odd mode waves generated in the magnetosphere. These fine phase relationships were observed when the stations were not under the substorm onset-site where the violent ionospheric electrojet was dominant, like the case shown in image f. It is also noteworthy to note that the start of the long-period waves before the onset was closely associated with the gradual intensification of the low-altitude AKR. This suggests that some magnetospheric disturbances were activated prior to the substorm onset, resulting in the MHD wave generation in the magnetosphere and intensification of the field-aligned acceleration (low-altitude AKR) in the M-I coupling region.

3.3.2. 16 April 1996 Event

[22] Figure 6 illustrates the detailed evolution of AKR and ground-based ULF pulsations. Figure 6a shows the *a-t* diagram of AKR for 15 minutes on 16 April 1996. AKR breakup occurred ~23:13 UT preceded by the gradual enhancement of low-altitude AKR from about 23:10 UT. The magnetogram at Kvistberg (L = 3.3) is shown in Figure 6b, where midlatitude Pi 2 pulsation began around 23:13 UT. From these two remote observations of the substorm, we can say the onset time of the substorm was 23:12:40–23:13:10 UT (indicated by the vertical rectangle in the figure).

[23] Figure 6c shows the ULF (dH/dt) data at Tjornes. The irregular pulsations that started around 23:11 UT are the high-latitude Pi 2 pulsations [e.g., *Olson*, 1999]. Around this time, Tjornes was at premidnight location (midnight in magnetic local time (MLT) is 23:45 UT at Tjornes). It is interesting that dH/dt data showed quasi-DC variation toward negative values with alternative oscillations. The simultaneous negative excursion of the dH/dt signal was also observed at the conjugate station, Syowa (not shown). To investigate the characteristics of this geomagnetic fluctuation, we analyzed ULF signals in terms of the band-pass ampligram. Figures 6d–6m show the band-pass components of dH/dt signal at Tjornes divided into ten period bands in the period range 2 to 100 seconds. Three ULF components related to the substorm onset are evident from this band-pass ampligram.

[24] Quasi-DC component: The dH/dt signal began to negatively decrease (quasi-DC variation) about 2 minutes before the substorm onset, roughly simultaneous with the gradual enhancement of low-altitude AKR. This is obvious from both the raw dH/dt data and from band-10 (Figure 6m), where a gradual decrease of the field began around 23:11 UT. This negative excursion of the derivative of the geomagnetic H-component ($d/d/t$ (dH/dt) < 0) suggests an exponential increase in the westward electrojet current in the ionosphere, induced by the exponential increase in the upward FAC. It should be also noted that the decrease in the quasi-DC component just before the onset seen in band-10 was again accelerated around the substorm onset, indicating the explosive reinforcement of FAC at the onset. This reinforced FAC would correspond to the upward current part of the substorm current wedge (SCW) system [e.g., *Akasofu*, 1972; *McPherron et al.*, 1973; *Lui*, 1996].

[25] Shorter period component: Short period components (less than 30 seconds) showed irregular variations, as seen in Figures 6d to 6f. The amplitudes of these fluctuations gradually increased starting almost simultaneously with the appearance of the quasi-DC component (blue areas in band-1 and -2). These fluctuations are interpreted as the noise component of the exponentially increasing FAC. Note that the amplitudes of this noise suddenly increased after the substorm onset (beige area in band-1 and -2). This is consistent with the signature of the tail-current disruption with violent fluctuations and/or fluctuations associated with the ionospheric Alfvén resonator [e.g., *Lysak*, 1991].

[26] MHD wave component: Two kinds of MHD waves related to substorm onset were observed. They seem to be excited in the magnetosphere because they showed in-phase oscillation between the conjugate stations (not shown). In the period range between 30 and 50 seconds (band-4 and -5), small-amplitude but continuous waves appeared around 23:11 UT (blue areas in band-4 and -5) nearly simultaneous with the appearance of the negative quasi-DC component (Figure 6c). The excitation of these waves prior to the substorm onset would be closely related to the gradual enhancement of the FAC driven in the near-Earth magnetosphere. At substorm onset, the wave amplitude was suddenly enhanced, and then showed damping after the onset (beige areas in band-4 and -5). Another wave component related to the substorm is the longer period pulsation with a large amplitude, as seen in band-7 to band-10 (note that the vertical axis for these components is twice that for components with shorter bands). This longer period oscillation was excited about 1 minute after the onset (beige areas in band-7 to -10) and consisted of a small number of wave trains.

4. Discussion

4.1. Summary of Observations

[27] Dual structure of auroral acceleration regions: Two sources of AKR were identified at substorm onsets from frequency spectrograms observed by Polar/PWI. One source is a low-altitude source corresponding to middle-frequency (MF) AKR, and the other is a high-altitude source corresponding to low-frequency (LF) AKR. The former appears in the substorm growth phase at altitudes from 4000 to 5000 km and intensifies a few minutes prior to the

substorm onset. In contrast, the high-altitude AKR appears abruptly with intense power in a higher and wider altitude range, 6000 to 12,000 km. The increase in its power is explosive (increasing 10,000 times with the growth time of 30 seconds), suggesting the abrupt growth of the parallel electric fields that cause bursty auroral electron beams. The source of the onset-associated high-altitude AKR is different from that of the preexisting low-altitude AKR, showing that the source is not a simple expansion from a preexisting AKR source but a newly developed one. This duality of AKR sources is a common feature of substorms. These findings of the vertical structure of the M-I coupling region and its dynamics at substorm onsets could not be made until the fine-resolution wave data from the Polar satellite, became available.

[28] The existence of two AKR sources suggests the existence of two types of field-aligned accelerations in the M-I coupling region during a substorm. On the basis of in-situ observations by the FAST satellite, *Ergun et al.* [2000] suggested that the parallel electric fields are concentrated in at least two locations: high-altitude $E_{//}$ near $\sim$1 R_E and low-altitude $E_{//}$ between $\sim$2000 and $\sim$5000 km along the magnetic field lines. The statistical study of the electric field distribution using in-situ E-field observations by the Polar satellite [*Mozer and Hull*, 2001] showed that the high-, middle-, and low-altitude electric field regions are roughly at 2.5–3 R_E, at 2–2.5 R_E, and below $\sim$2 R_E geocentric, respectively. These in-situ observations are not necessarily consistent with the present study. This may be partly because their analyses were essentially statistical ones based on long-term observations in contrast to our remote and temporal observations.

[29] AKR breakup: AKR breakup is defined in this study as the explosive development of a high-altitude AKR source at the time of an auroral breakup, which suggests the abrupt formation of an acceleration region above a preexisting and fairly stable low-altitude acceleration region. The explosive growth of the high-altitude acceleration in a very short time implies a local and coherent development of acceleration. Auroral observations by means of recent photometers with high-time resolution have revealed the detailed development of auroral breakup. *Friedrich et al.* [2001] reported that the auroral expansion phase is composed of three stages and that the first explosive onset takes place within tens of seconds before the poleward motion of 557.7-nm emissions. *Mende et al.* [2007] examined one example of substorm using the THEMIS ground-based observations and showed that it took 27 seconds from arc brightening to auroral breakup. This breakup time seems to be consistent with the growth time for the AKR breakup ($\sim$30 seconds).

[30] Pre-onset activity of AKR and auroral arc: AKR breakups are usually preceded within 1–3 minutes by the appearance and/or gradual enhancement of low-altitude AKR, which can be seen in Figures 1 to 6. This suggests that the explosive buildup of the high-altitude electric field takes place in the course of the gradual growth of low-altitude acceleration, in other words, low-altitude acceleration is a necessary condition for the ignition of high-altitude bursty acceleration.

[31] It was also shown in this study (as seen in Figures 3 and 4) that, almost concurrently with the beginning of the low-altitude AKR, the auroral arc exhibited the pre-onset activity prior to the auroral and AKR breakup. This suggests that the low-altitude acceleration along the auroral oval is responsible for the activation of both the longitudinally elongated auroral arc and the low-altitude AKR before the onset. Recent ground-based auroral observations disclosed the detailed behavior of auroral features around substorm onset. *Friedrich et al.* [2001] reported a case in which there was a period of emission intensification 4 min prior to the poleward movement. *Lyons et al.* [2002] showed that the intensity of the breakup arc increases monotonically for the few minutes prior to the substorm onset and then increases explosively. These observations would correspond to the present pre-onset activity of the auroral arc and the low-altitude AKR.

[32] ULF around substorm onset: The ULF signals (dH/dt) from the search-coil magnetometer at ground presented very interesting behaviors prior to auroral and AKR breakup. The quasi-DC component of dH/dt showed a gradual negative excursion almost concurrent with the enhancement of low-altitude AKR before the onset. The negative excursion suggests the exponentially increasing westward auroral electrojet current induced by the exponentially increasing upward FAC. At auroral and AKR breakups, the decrease in this component further accelerated indicating the sudden reinforcement of the FAC. This quasi-DC variation before a substorm has remained unnoticed except by *Kepko et al.* [2004], who described a high-latitude magnetic precursor to the substorm onset.

[33] In spite of the few reports of this phenomenon, we can show how common these phenomena are in the night side auroral region. Figure 7 shows typical records of dH/dt component from the search-coil magnetometer for a 4-week period (16 April to 13 May 1996) at the Tjornes-Syowa conjugate-pair stations. The arrow above each panel shows the onset of the midlatitude Pi 2 pulsation detected at the SAMNET stations. Many negative quasi-DC variations were found prior to the onset (hatched portions in the figure). The reason why these common phenomena were not previously noticed is probably that most examinations of ULF phenomena have been done using high-pass filtered data from an ordinary magnetometer.

[34] As shown in Figure 6, the high-latitude Pi 2 can be described in terms of both the short-period (less than 30 seconds) irregular fluctuation and MHD waves which show the in-phase oscillation between the conjugate-pair stations. The former is characterized by its gradual amplification as the quasi-DC component intensifies before the onset and its sudden reinforcement immediately at auroral and AKR breakup. This component can be attributed to the fluctuation in the ionospheric current that connects to FAC. The MHD waves are rather smooth and continuous and can be classified into two components. The first component belongs to Pc 3 pulsation with a period of 30–60 seconds. A remarkable characteristic of this pulsation is that it starts almost simultaneously with the appearance of the quasi-DC component of dH/dt and low-altitude AKR prior to the onset. These waves may correspond to the kinetic ballooning instability (KBI) in the plasma sheet during the growth phase, as discussed by *Cheng and Zaharia* [2004]. The other MHD waves appear immediately after substorm onset with a longer period (more than 80 seconds) and are characterized by a shorter duration and 1–2 pulse trains.

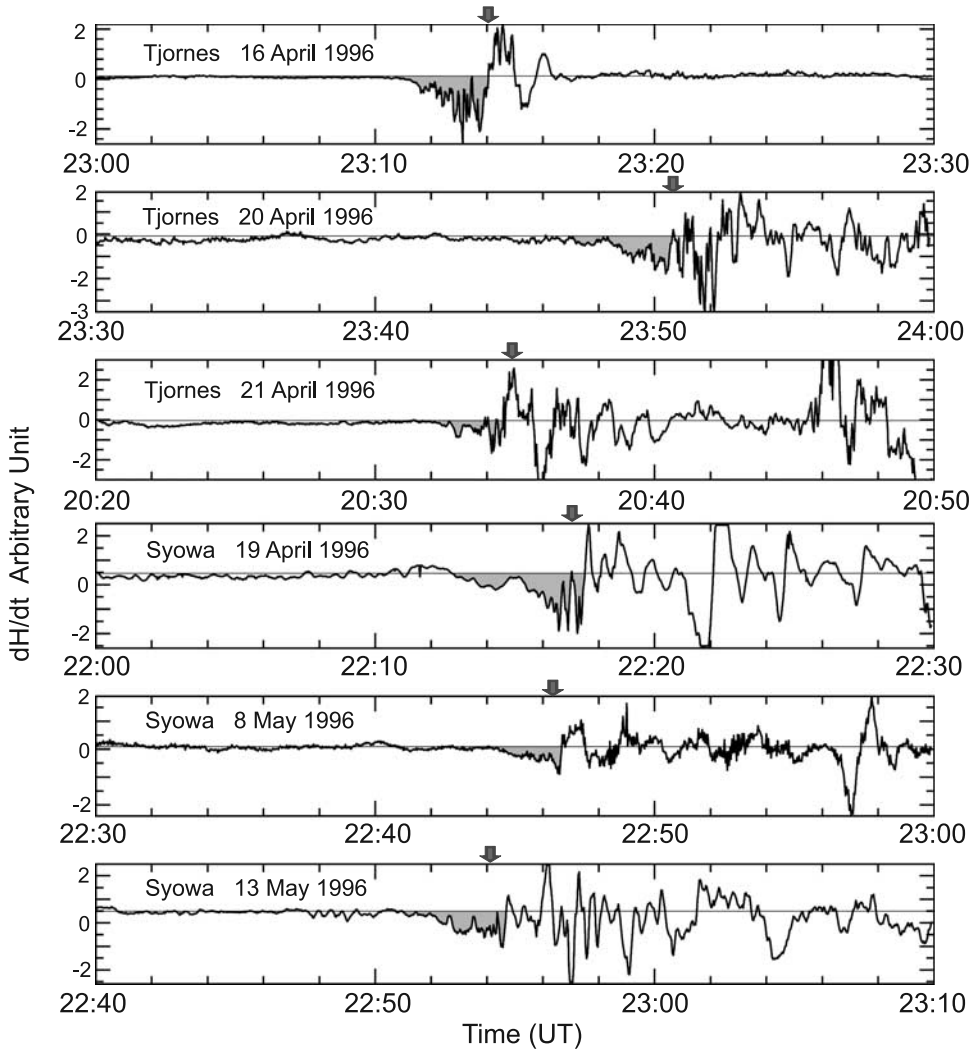

Figure 7. Negative excursion of d*H*/d*t* signals before substorm onset. The hatched portion in each panel indicates quasi-DC variation in d*H*/d*t* signal toward negative prior to onset. The arrow above each figure indicates onset of midlatitude Pi 2 pulsation detected by SAMNET stations. Examples shown were gathered during 4 weeks (16 April to 13 May 1996) at Tjornes-Syowa conjugate-pair stations.

4.2. Formation of Field-Aligned Acceleration at Around Substorm Onset

[35] The scenario for the formation of field-aligned acceleration at substorm onset is required to explain the essential evidence presented in this study: (1) separate acceleration regions at lower (4000–5000 km) and higher (6000–12,000 km) altitudes, (2) gradual intensification of low-altitude acceleration prior to AKR onset, and (3) explosive growth (within 30 seconds) of a high-altitude acceleration region at onset.

[36] The large-scale quasi-static field-aligned electric field has been discussed as a self-consistently formed electrostatic potential structure due to the anisotropic magnetospheric plasma distribution, such as quasi-static double layers [e.g., *Block*, 1972; *Ergun et al.*, 2004], electrostatic shocks [e.g., *Swift*, 1975], and the magnetic mirror process [e.g., *Chiu and Schulz*, 1978]. The low-altitude acceleration region described in this paper belongs to this category of acceleration process. *Chiu and Schulz* [1978] estimated the potential structure along the auroral field line on the basis of the magnetic mirror process. One of their results is shown in the form of an electric field profile in Figure 8 (curve a), where the electric field peaks in a rather narrow altitude range (3000–5000 km) consistent with the present study. The observed pre-onset phenomena can also be understood by the enhancement of this electric field. At the end of the substorm growth phase, the tail current is increased [e.g., *McPherron*, 1972; *Ohtani et al.*, 1992, 2000] and the low-altitude inverted-V electric field along the auroral oval is enhanced. The electron beams accelerated by this low-altitude electric field activate the auroral arc on the oval and also generate and/or intensify the low-altitude AKR. According to the equation by *Knight* [1973], the FAC is also enhanced which results in the intensification of the westward electrojet current in the ionosphere, inducing a negative excursion of the quasi-DC d*H*/d*t* component with short-period fluctuation (Figures 6d and 6e). The feedback system between the magnetosphere and ionosphere may work in this phase, leading to still stronger FAC, through the mechanism such as feedback instability [*Sato*, 1978;

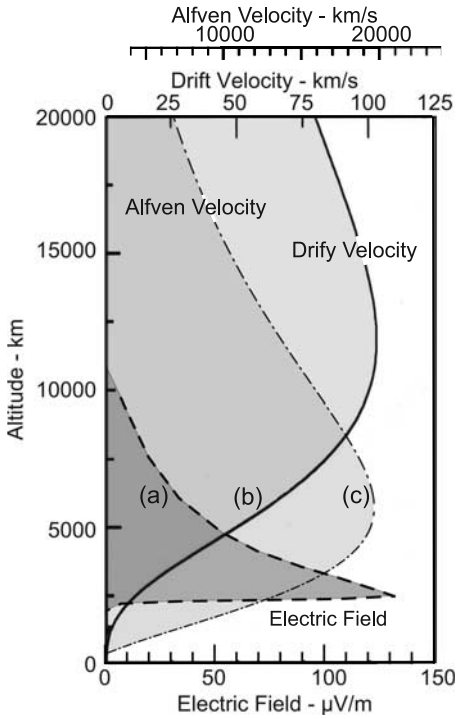

Figure 8. (a) Altitude distribution of field-aligned electric field derived from magnetic mirror process by *Chiu and Schulz* [1978]. (b) Altitude profile of drift velocity of FAC electron [*Morioka et al.*, 2005]. (c) Altitude profile of Alfvén velocity. Curves (b) and (c) are based on the empirical electron density model along the $L = 7$ field line.

Watanabe et al., 1993]. Present observations showed that these precursor-like processes usually occur 1–3 minutes before substorm onset. This period would be intimately connected with the ''explosive growth phase'' in the near-Earth plasma sheet suggested by *Ohtani et al.* [1992, 2000].

[37] The drastic appearance of a high-altitude acceleration region at substorm onset means that the buildup of the region is due to the explosive acceleration process on the field line of the local onset site. Among various theories for the generation of the field-aligned acceleration [*Borovsky*, 1993], the time-dependent mechanisms can be categorized into (1) anomalous resistivity as the consequence of wave instabilities such as current driven instability [*Kindel and Kennel*, 1971], (2) microscopic double layers such as ion-acoustic double layers [*Sato and Okuda*, 1981] and electron holes [*Pottelette and Treumann*, 2005], (3) kinetic Alfvén waves [e.g., *Lysak and Lotko*, 1996; *Lysak and Song*, 2003], and (4) shear flow evolution in the plasma sheet which results in the field-aligned acceleration [e.g., *Birn and Hesse*, 1991]. Although the present observations do not enable to identify the most probable mechanism for the high-altitude acceleration, the mechanism is restricted, in addition to the explosive growth to complete the acceleration (within 30 seconds), to have an effective acceleration altitude of 6000–12000 km. In Figure 8, the estimated altitude profile of the drift velocity of the FAC electrons [*Mozer et al.*, 1977; *Morooka and Mukai*, 2003] and the Alfvén velocity along the $L = 7$ field line are shown (curves b and c) using the vertical electron density distribution on the dusk side (21 MLT) observed by the Akebono satellite [*Sato*, 1998; *Morioka et al.*, 2005]. The drift velocity of FAC carrier electrons has a broad maximum at around 10,000 km. This seems to be preferable to the observed high-altitude acceleration and suggests that the mechanism for the high-altitude acceleration is closely related to the FAC intensity and its altitude profile. The estimated Alfvén velocity shows a peak at around 5000 km (curve c in Figure 8), indicating that the ionospheric Alfvén resonator (IAR) [*Polyakov and Rapoport*, 1981] forms below this altitude. This implies that Alfvén waves are not effective for the high-altitude acceleration.

[38] The critical issue for substorm onset is the causality between the sudden formation of the high-altitude field-aligned acceleration in the M-I coupling region and the abrupt disruption of the near-Earth tail-current in the plasma sheet. Does the sudden acceleration in the M-I coupling region ignite the tail-current disruption or does the tail-current disruption in the plasma sheet induce the ionospheric acceleration? In the context of the present observation, it is not unreasonable to assert that the sudden formation of the high-altitude field-aligned acceleration in the M-I coupling region ignites the tail-current disruption when the intensified acceleration in the M-I coupling region rapidly induces and accelerates the inflow of the tail-current into the ionosphere. In this case, massive current is quickly injected into the ionosphere from the plasma sheet; that is, the tail-current is disrupted. The advantage of this hypothesis is that substorm onset is self-consistently determined through interaction between the magnetosphere and ionosphere.

5. Conclusions

[39] We have investigated the dynamical behavior of AKR in connection with the auroral particle acceleration during substorm onsets, using high-time-resolution wave spectrograms provided by Polar/PWI electric field observations. At the substorm onset, AKR showed explosive development at higher altitudes (6000–12,000 km) above a preexisting low-altitude AKR source (4000–5000 km). This AKR breakup suggests the abrupt formation of a new high-altitude field-aligned acceleration region at the substorm onset. The growth time of the new acceleration region is very short (increasing amplitude of 10,000 times within 30 seconds), suggesting a local and explosive development. The low-altitude AKR showed gradual enhancement 1–3 minutes prior to the AKR breakup. This suggests that the explosive formation of the high-altitude electric field takes place in the course of the growing low-altitude acceleration; in other words, the development of a low-altitude acceleration region is a necessary condition for the ignition of the high-altitude bursty acceleration.

[40] Before the substorm onset, the quasi-DC component of dH/dt (ULF) signal showed negative excursion that was almost synchronized with the start of the gradual enhancement of the low-altitude AKR, showing precursor-like behavior for the substorm. This negative variation of dH/dt suggests an exponentially increasing ionospheric current induced by the upward FAC. At the substorm onset, the decrease in the quasi-DC variation of dH/dt is further accelerated, indicating a sudden enhancement of the FAC, that is, the current disruption.

[41] **Acknowledgments.** We are grateful to K. Shiokawa, R. Kataoka, A. Kadokura, N. Sato, and H. Yamagishi for their useful comments and discussions. The authors would like to thank the Polar/PWI team (principal investigator is D. Gurnett). The CANMOS magnetometer data from Victoria was collected by the Geological Survey of Canada. The 1-second resolution geomagnetic data were observed by the Kakioka Magnetic Observatory, Japan Meteorological Agency, and provided through the WDC-2 for Geomagnetism at Kyoto University, Japan. The geomagnetic data from Syowa-Tjornes conjugate-pair stations were kindly provided by the Auroral Data Center at the National Institute of Polar Research, Japan. We thank the SAMNET team for the magnetometer data. SAMNET is operated by Lancaster University and is funded by STFC. We acknowledge L. Cogger, the principal investigator of the CANOPUS ASI at Gillam, and the Canadian Space Agency, for producing the ASI data used in this study. We also thank J. Dowell of the University of Iowa for providing the Polar/PWI data and her very efficient programming support.

[42] Wolfgang Baumjohann thanks Michael Kaiser and another reviewer for their assistance in evaluating this paper.

References

Akasofu, S.-I. (1964), The development of the auroral substorm, *Planet. Space Sci.*, *12*, 273–282.

Akasofu, S.-I. (1972), Magnetospheric substorm, a model, in *Solar Terrestrial Physics, Part III*, edited by Dyer, p. 131, D. Reidel Norwell, Hingham, Mass.

Anderson, R. R., et al. (1997), Observation of low frequency terrestrial type III bursts by Geotail and WIND and their association with isolated geomagnetic disturbances detected ground and space-bone instruments, in *Planetary Radio Emissions IV, Proc. Graz Conf.*, edited by H. O. Rucker, S. J. Bauer, and A. Lecacheux, pp. 241–250, Austrian Academy of Sciences Press, Vienna, Austria.

Anderson, R. R., et al. (1998), Geotail, Polar, CANOPUS ISTP associated geosynchronous satellite observations of plasma wave emissions and related magnetospheric phenomena during substorms, in *SUBSTORM-4*, edited by S. Kokubun and Y. Kamide, pp. 567–572, Terra Sci., Tokyo.

Arnoldy, R. L., P. B. Lewis, and P. O. Isaacson (1974), Field aligned auroral electron fluxes, *J. Geophys. Res.*, *79*(28), 4208–4221.

Baker, D. N., T. I. Pulkkinen, V. Angelopoulos, W. Baumjohann, and R. L. McPherron (1996), Neutral line model of substorms: Past results and present view, *J. Geophys. Res.*, *101*(A6), 12,975–13,010.

Birn, J., and M. Hesse (1991), The substorm current wedge and field-aligned currents in MHD simulation of magnetotail reconnection, *J. Geophys. Res.*, *96*(A2), 1611–1618.

Block, L. P. (1972), Potential double layers in the ionosphere, *Cosmic Electrodyn.*, *3*, 349–376.

Borovsky, J. E. (1993), Auroral arc thickness as predicted by various theories, *J. Geophys. Res.*, *98*(A4), 6101–6138.

Cheng, C. Z., and S. Zaharia (2004), MHD ballooning instability in the plasma sheet, *Geophys. Res. Lett.*, *31*, L06809, doi:10.1029/2003GL018823.

Chiu, Y. T., and M. Schulz (1978), Self-consistent particle and parallel electrostatic field distributions in the magnetospheric-ionospheric auroral region, *J. Geophys. Res.*, *83*(A2), 629–642.

de Feraudy, H., J. Hanasz, R. Schreiber, G. Parks, M. Brittnacher, S. Perraut, J. A. Sauvaud, F. Lefeuvre, and M. M. Mogilevsky (2001), AKR bursts and substorm field line excitation, *Phys. Chem. Earth (C)*, *26*, 151–159.

Desch, M. D., and W. M. Farrell (2000), Terrestrial LF burst: Escape paths and wave intensification, in *Radio Astronomy at Long Wavelengths*, edited by R. G. Stone et al., pp. 205–211, AGU, Washington, D. C.

Delory, G. T., et al. (1998), FAST observations of electron distributions within AKR source regions, *Geophys. Res. Lett.*, *25*(12), 2069–2072.

Ergun, R. E., et al. (1998), FAST satellite wave observations in the AKR source region, *Geophys. Res. Lett.*, *25*(12), 2061–2064.

Ergun, R. E., C. W. Carlson, J. P. McFadden, G. T. Delory, R. J. Strangeway, and P. L. Pritchett (2000), Electron-cyclotron maser driven by charged-particle acceleration from quasi-static field-aligned potentials, *Astrophys. J.*, *538*, 456–466.

Ergun, R. E., L. Anderson, D. S. Main, and Y.-J. Su (2002), Parallel electric fields in the upward current region of the aurora: Indirect and direct observations, *Phys. Plasma*, *9*, 3685–3694.

Ergun, R. E., L. Anderson, D. Maun, and Y.-J. Su (2004), Auroral particle acceleration by strong double layers: The upward current region, *J. Geophys. Res.*, *109*, A12220, doi:10.1029/2004JA010545.

Evans, D. S. (1974), Precipitating electron fluxes formed by a magnetic field-aligned potential difference, *J. Geophys. Res.*, *79*(19), 2853–2858.

Friedrich, E., J. C. Samson, I. Voronkov, and G. Rostorker (2001), Dynamics of the substorm expansive phase, *J. Geophys. Res.*, *106*(A7), 13,145–13,163.

Frank, L. A., and K. L. Ackerson (1971), Observations of charged particle precipitation into the auroral zone, *J. Geophys. Res.*, *76*(16), 3612–3643.

Gurnett, D. A., et al. (1995), The Polar plasma wave instrument, *Space Sci. Rev.*, *71*, 597–622.

Hanasz, J., H. de Feraudy, R. Schreiber, G. Parks, M. Brittnacher, M. M. Mogilevsky, and T. V. Romantsova (2001), Wideband bursts of auroral kilometric radiation and their association with UV auroral bulges, *J. Geophys. Res.*, *106*(A3), 3859–3871.

Janhunen, P., A. Ollson, J. Hanasz, C. T. Russell, H. Laakso, and J. C. Samson (2004), Different Alfvén wave acceleration processes of electrons in substorms at ~4–5 R_E and 2–3 R_E radial distance, *Ann. Geophys.*, *22*, 2213–2227.

Kaiser, M. L., and J. K. Alexander (1977), Relationship between auroral substorms and the occurrence of terrestrial kilometric radiation, *J. Geophys. Res.*, *82*(32), 5238–5286.

Kaiser, M. L., M. D. Desch, W. M. Farrell, J.-L. Steinberg, and M. J. Reiner (1996), LF band terrestrial radio bursts observed by Wind/WAVES, *Geophys. Res. Lett.*, *23*(10), 1283–1286.

Kepko, L., M. G. Kivelson, R. L. McPherron, and H. E. Spence (2004), Relative timing of substorm onset phenomena, *J. Geophys. Res.*, *109*, A04203, doi:10.1029/2003JA010285.

Kindel, J. M., and C. F. Kennel (1971), Topside current instabilities, *J. Geophys. Res.*, *76*(13), 3055–3078.

Knight, S. (1973), Parallel electric fields, *Planet. Space Sci.*, *21*, 741–750.

Liou, K., C.-I. Meng, A. T. Lui, and P. T. Newell (1999), On relative timing in substorm onset signatures, *J. Geophys. Res.*, *104*(A10), 22,807–22,817.

Liou, K., C.-I. Meng, A. T. Lui, and P. T. Newell (2000), Auroral kilometric radiation at substorm onset, *J. Geophys. Res.*, *105*(A11), 25,325–25,331.

Lui, A. T. Y. (1996), Current disruption in the Earth's magnetosphere: Observations and models, *J. Geophys. Res.*, *101*(A6), 13,067–13,088.

Lui, A. T. Y., et al. (1992), Current disruption in the near-earth neutral sheet region, *J. Geophys. Res.*, *97*(A2), 1461–1480.

Lyons, L. R. (1995), A new theory for magnetospheric substorms, *J. Geophys. Res.*, *100*(A10), 19,069–19,081.

Lyons, L. R., I. O. Voronkov, E. F. Donovan, and E. Zesta (2002), Relation of substorm breakup arc to other growth-phase auroral arcs, *J. Geophys. Res.*, *107*(A11), 1390, doi:10.1029/2002JA009317.

Lysak, R. L. (1991), Feedback instability of the ionospheric resonant cavity, *J. Geophys. Res.*, *96*(A2), 1553–1568.

Lysak, R. L., and W. Lotko (1996), On the kinetic dispersion relation for shear Alfvén waves, *J. Geophys. Res.*, *101*(A3), 5085–5094.

Lysak, R., and Y. Song (2003), Kinetic theory of the Alfvén wave acceleration of auroral electrons, *J. Geophys. Res.*, *108*(A8), 8005, doi:10.1029/2002JA009406.

McPherron, R. L. (1972), Substorm related changes in the geomagnetic tail: The growth phase, *Planet. Space Sci.*, *20*, 1521–1539.

McPherron, R. L., C. T. Russell, and M. P. Aubry (1973), Satellite studies of magnetospheric substorms on August 15, 1968. 9: Phenomenological model for substorms, *J. Geophys. Res.*, *78*(16), 3131–3149.

Mende, S. B., et al. (2007), Determination of substorm onset timing and location using the THEMIS ground based observations, *Geophys. Res. Lett.*, *34*, L17108, doi:10.1029/2007GL030850.

Meng, C.-I., and K. Liou (2004), Substorm timings and timescales: A new aspect, *Space Sci. Rev.*, *113*, 41–75.

Mizera, P. F., and J. F. Fennell (1977), Signatures of electric fields from high and low altitude particles distributions, *Geophys. Res. Lett.*, *4*(8), 311–314.

Morioka, A., H. Oya, and S. Miyatake (1981), Terrestrial kilometric radiation observed by satellite Jikiken (Exos-B), *J. Geomagn. Geoelectr.*, *33*, 37–62.

Morioka, A., Y. S. Miyoshi, F. Tsuchiya, H. Misawa, A. Kumamoto, H. Oya, H. Matsumoto, K. Hashimoto, and T. Mukai (2005), Auroral kilometric radiation activity during magnetically quiet periods, *J. Geophys. Res.*, *110*, A11223, doi:10.1029/2005JA011204.

Morioka, A., Y. Miyoshi, F. Tsuchiya, H. Misawa, T. Sakanoi, K. Yumoto, R. R. Anderson, J. D. Menietti, and E. F. Donovan (2007), Dual structure of auroral acceleration regions at substorm onsets as derived from AKR spectra, *J. Geophys. Res.*, *112*, A06245, doi:10.1029/2006JA012186.

Morooka, M., and T. Mukai (2003), Density as a controlling factor for seasonal and latitudinal variations of the auroral particle acceleration region, *J. Geophys. Res.*, *108*(A7), 1306, doi:10.1029/2002JA009786.

Mozer, F. S., C. W. Carlson, M. K. Hudson, R. B. Torbert, B. Paraday, and J. Yateau (1977), Observations of paired electrostatic shocks in the polar magnetosphere, *Phys. Rev. Lett.*, *38*, 292–295.

Mozer, F. S., and A. Hull (2001), Origin and geometry of upward electric fields in the auroral acceleration region, *J. Geophys. Res.*, *106*(A4), 5763–5778.

Ohtani, S., K. Takahashi, L. J. Zanetti, T. A. Potemura, and R. W. McEntire (1992), Initial signatures of magnetic field and energetic particle fluxes at tail reconfiguration: Explosive growth phase, *J. Geophys. Res.*, *97*(A12), 19,311–19,324.

Ohtani, S., A. T. Y. Lui, K. Takahashi, D. G. Mitchell, and T. Sarris (2000), Ion dynamics and tail current intensification prior to depolarization: The June 1, 1985, event, *J. Geophys. Res.*, *105*(A11), 25,233–25,246.

Olson, J. V. (1999), Pi2 pulsations and substorm onsets: A review, *J. Geophys. Res.*, *104*(A8), 17,499–17,520.

Olsson, A., P. Janhunen, J. Hanasz, M. Mogilevsky, S. Perraut, and J. D. Menietti (2004), Observational study of generation conditions of substorm-associated low-frequency AKR emissions, *Ann. Geophys.*, *22*, 3571–3582.

Polyakov, S., and V. O. Rapoport (1981), Ionospheric Alfvén resonator, *Geomagn. Aeron.*, *21*, 816–822.

Pottelette, R., R. A. Treumann, and M. Berthomier (2001), Auroral plasma turbulence and cause of auroral kilometric radiation fine structure, *J. Geophys. Res.*, *106*(A5), 8465–8476.

Pottelette, R., and R. A. Treumann (2005), Electron holes in the auroral upward current region, *Geophys. Res. Lett.*, *32*, L12104, doi:10.1029/2005GL022547.

Saito, T., K. Yumoto, and Y. Koyama (1976), Magnetic pulsation Pi 2 as a sensitive indicator of magnetospheric substorm, *Planet. Space Sci.*, *24*, 1025–1029.

Sato, T. (1978), A theory of quiet aurora arcs, *J. Geophys. Res.*, *83*(A3), 1042–1048.

Sato, T., and H. Okuda (1981), Numerical simulations on ion acoustic double layers, *J. Geophys. Res.*, *86*(A5), 3357–3368.

Sato, Y. (1998), A study on electron density distributions at high latitude, master thesis, Tohoku Univ. Sendai, Japan.

Shiokawa, K., et al. (1998), High-speed ion flow, substorm current wedge, and multiple Pi 2 pulsations, *J. Geophys. Res.*, *103*(A3), 4491–4507.

Shelley, E. G., R. D. Sharp, and R. G. Johnson (1976), Satellite observations of an ionospheric acceleration mechanism, *Geophys. Res. Lett.*, *3*(11), 654–656.

Steinberg, J.-L., C. Lacombe, and S. Hang (1988), A new component of terrestrial radio emission observed from ISEE-3 and ISEE-1 in the solar wind, *Geophys. Res. Lett.*, *15*(2), 176–179.

Steinberg, J.-L., S. Hoang, and J.-M. Bosqued (1990), Isotropic terrestrial kilometric radiation—A new component of the earth's radio emission, *Ann. Geophys.*, *8*, 671–685.

Swift, D. W. (1975), On the formation of auroral arcs and acceleration of auroral electrons, *J. Geophys. Res.*, *80*(16), 2096–2108.

Torr, M. R., et al. (1995), A far ultraviolet image for the International Solar-Terrestrial Physics' Mission, *Space Sci. Rev.*, *71*, 329–383.

Yumoto, K., et al. (1994), Correlation of high- and low-latitude Pi2 magnetic pulsations observed at 210 magnetic meridian chain stations, *J. Geomagn. Geoelectr.*, *46*, 925–935.

Watanabe, T., H. Oya, K. Watanabe, and T. Sato (1993), Comprehensive simulation study on local and global development of auroral arcs and field-aligned potentials, *J. Geophys. Res.*, *98*(A12), 21,391–21,407.

R. R. Anderson and J. D. Menietti, Department of Physics and Astronomy, University of Iowa, Iowa City, IA 52242, USA.

E. F. Donovan and E. Spanswick, Department of Physics and Astronomy, University of Calgary, Calgary, Alberta, Canada AB T2N 124.

F. Honary, Department of Communication Systems, Lancaster University, Lancaster LA14YW, UK.

H. Misawa, A. Morioka, and F. Tsuchiya, Planetary Plasma and Atmospheric Research Center, Tohoku University, Sendai 980-8578, Japan, (morioka@pparc.geophys.tohoku.ac.jp)

Y. Miyoshi, Solar-Terrestrial Environment Laboratory, Nagoya University, Nagoya 464-8601, Japan.

G. K. Parks, Space Sciences Laboratory, University of California, Berkeley, CA 94720, USA.

K. Yumoto, Space Environment Research Center, Kyushu University, Fukuoka 812-8581, Japan.